Numerical Identification of Optimum Process Parameters for Combined Deep Drawing and Electromagnetic Forming*

M. Stiemer[1], F. Taebi[2], M. Rozgic[1], R. Appel[1]

[1] Institute for the Theory of Electrical Engineering, Helmut-Schmidt-University / University of the Federal Armed Forces Hamburg, Germany
[2] Chair of Scientific Computation, TU-Dortmund, Germany

Abstract

In this paper, a method is presented for the virtual process design of combinations of deep drawing and electromagnetic forming. With suitably chosen parameters, such process combinations of a quasi-static and an impulse forming process extend forming limits of classical, purely quasi-static forming. To determine parameters leading to the desired forming result, a numerical optimization algorithm is employed. The parameters to be adjusted comprise parameters of the triggering current, such as frequency, amplitude, damping, etc., geometric parameters of the tool coil and parameters of the deep drawing process, as, e.g., drawing radii or tribological parameters. To reduce the required number of evaluations of the target function, a gradient based numerical optimization scheme is employed following directions of decent in the parameter space. The quality of a given parameter set is determined by computing the distance of the simulated forming result to the prescribed ideal shape via a finite element simulation. Forming limits are incorporated by so called forming limit surfaces as constraints to the optimization process, considering rate dependence and prestrain in the second impulse forming step.

Keywords

Electromagnetic forming, Process combinations, Numerical optimization

This work is based on the results of the research project PAK343-2; the authors would like to thank the German Research Foundation (DFG) for its financial support. Further, the authors are indebted to the Institute of Forming Technology and Lightweight Construction (IUL) at the TU-Dortmund, particularly to Koray Demir, for providing the experimental data this work is based on.

1 Introduction

Deep drawing is one of the most frequently utilized industrial forming methods. Usually it is driven by the pressure exerted on a metal sheet by a punch. Forming is guided by a die and the material's flow is controlled by the blank holder force, the radius of the drawing ring at the flange, the bottom radius of the punch, the geometrical details of the drawing ring, the punch, and the die, and finally the friction between the work piece and the tool. The material flow of the sheet metal results from stretch-compression loading and stretch-bending loading or a combination of both. Deep drawing can be considered as a quasi-static forming process, i.e., inertial forces need not be considered. While many forming operations can be carried out by deep drawing, recent industrial requirements aim at forming methods with allow for a higher material formability. On the one hand this is a consequence of an interest in high-tensile materials, particularly for safety reasons. On the other hand the demand for light-weight constructed work pieces requires forming methods for more complicated geometries. In addition to this, the increasing competition in forming technology leads to the demand of more efficient production methods, particularly allowing for a reduction of production time and costs. Deep drawing on its own has not the potential to meet all these requirements. Using deep drawing as part of a process chain may help to extend forming limits. However, increased production time and costs have to be avoided at the same time. Therefore, integration of post-processing steps into the deep-drawing process is desirable. An option to meet both demands is combining deep drawing with electromagnetic forming.

Electromagnetic forming (EMF) is an impulse forming method in which strain rates over 1000 s^{-1} are achieved. It is driven by the Lorentz force, a material body force that results from the interaction of a pulsed magnetic field with eddy currents induced in the work piece by the magnetic field itself. The energy transferred by the Lorentz force is, however, not immediately transformed into plastic work. A great portion of it is stored as kinetic energy in the work piece, which then leads to deformation by inertial forces [1]. The magnetic field is generated by a tool coil adjacent to the work piece, which is excited by the discharging current of a capacitor bank. Typically, a current of several 10000 Ampère is generated within a time comparable to 10 µs, leading to magnetic flux densities in the order of 1-10 Tesla in the gap between tool coil and work piece. The whole forming process takes about 100 µs. As an individual forming process, EMF has already been scientifically studied in the 1960's, as described, e.g., by [2]. EMF possesses a huge potential to extend forming limits of classical techniques, particularly as part of a process chain [3]. In such a combination, all advantages of this forming method can take effect: Above all, an increased formability enables the extension of classical forming limits (e.g., [3,4]). Further, by a suitable design of the tool coil, loads can be applied locally and, hence, the spectrum of applicable load distributions is enormously extended. Next, tool coils can often completely be integrated into other forming tools, such that fully integrated multi-stage process combinations become possible (e.g., Figure 4 on the left hand side). Finally, the process only takes about 100 µs, such that the additional time required for a subsequent electromagnetic calibration step can be neglected. For detailed information as well as recent results on EMF and its use in process chains we refer to [5].

Recent experimental results show that such process combinations, indeed, lead to an extension of classical forming limits (e.g., [3] or [4]). As an example, compare Figure 1 and Figure 2. These show results of experiments carried out at the Institute of Forming

Technology and Lightweight Construction (IUL) at the TU-Dortmund (e.g., [4]). The right hand side of Figure 1 shows a forming limit diagram determined after a single deep drawing step. The left hand side of Figure 2 displays the corresponding diagram after a subsequent step of electromagnetic forming. Obviously, in the area of combined forming an amount of stretch has been achieved after EMF that exceeds the quasi-static formability. Forming limit diagrams are a frequently used indicator for material formability in quasi-static forming methods. In these diagrams the two principal strains (Eigenvalues of the true- or Hencky strain) in the sheet metal plane are compared to each other. In a diagram with the second principal Hencky strain on the abscissa (minor strain) and the first principal strain on the ordinate (major strain), a curve is inserted separating stress states leading to material failure from those without damage. To determine this curve, it is observed, when fracture occurs first. Although in deep drawing mechanical failure is usually defined via necking, we consider the forming limit curve for fracture, since we are interested in a comparison to high speed forming limits: In the case of the high strain rates typical of electromagnetic forming, emerging material failure cannot be observed accurately enough to capture necking before fracture occurs. To achieve consistency in the performed simulations and experiments we, hence, focus on fracture. Moreover, experimental data obtained so far give no information if necking at high strain rates occurs at all. It is remarkable that a similar discussion has arisen in a completely different field of forming technology: In single point incremental forming, it has also been impossible to clarify whether necking occurs before fracture so far. This discussion has, among others, led to the theory of fracture forming lines (see [6]).

Obviously, the construction of a forming limit curve depends on a very particular load situation, which does not apply if prestrain and rate dependence have a significant influence on the forming result. This is the reason, why classical forming limit diagrams cannot be used for the prediction of forming limits in case of nonlinear load paths or dynamic loading. We will address this issue in Chapter 3.

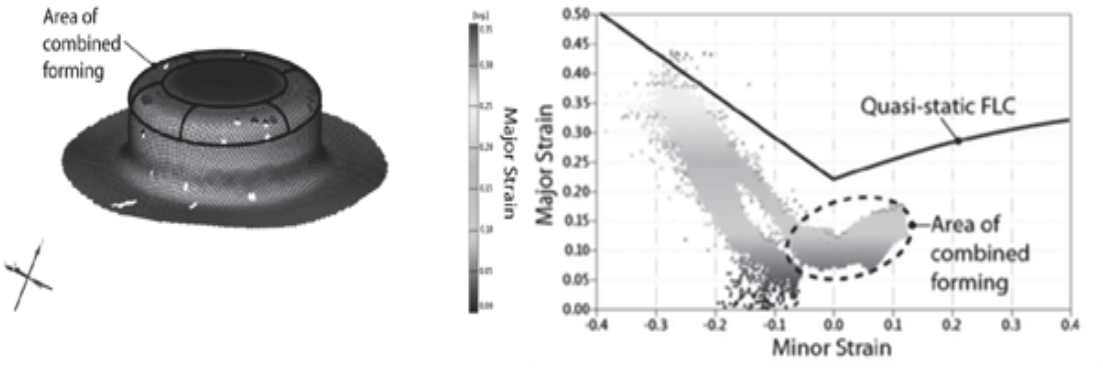

***Figure 1**: Right: Major and minor strain after deep drawing for the grid points marked on the surface of a work piece as displayed on the left. Brightness is related to major strain in both diagrams [4].*

Figures 1 and 2 have been produced by the ARGUS-system (Gesellschaft für OptischeMesstechnik). The principle idea to extend quasi-static forming limits is now to leave those load paths relevant in deep drawing and replace them by highly nonlinear and

strain-rate-dependent ones, as demonstrated in the preceding example. Experimental results show, however, that process parameters have to be carefully adjusted to gain an increase in formability with this approach. Hence, it is desirable to be able to predict those parameters that lead to an increased formability. Moreover, such a method reduces expensive experiments and development time for new products. This is a motivation for the use of numerical methods to identify suited process parameters leading to an extended formability.

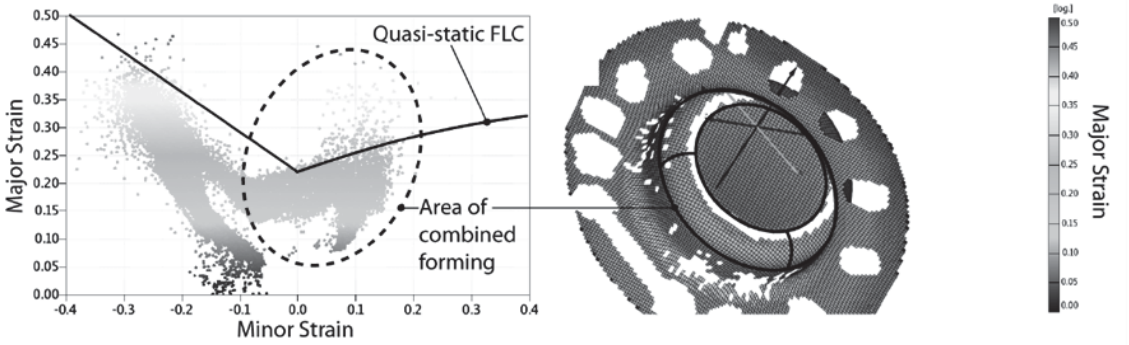

Figure 2: *Left: Major and minor strain after EMF for grid points marked on the surface of the work piece (brightness according to major strain). Right: Corresponding distribution of major strain on the work piece (same brightness scale) [4].*

2 Parameter Identification and Mathematical Optimization

The identification of optimum process parameters for process combinations as described in the introduction is based on the following three pillars:

- A finite element simulation of all steps of the combined process, i.e., of deep drawing and of EMF. It provides data required for the computation of the target function, rating the quality of the forming result.
- A numerical optimization method, which iteratively selects parameters that lead to better values of the target function. It uses information provided by the values of the target function known so far.
- A method to implement forming limits relevant for the chosen load paths as constraints for the optimization method. Particularly, prestrain and rate dependence have to be considered.

We will discuss the third point in Chapter 3, while the first and the second are considered now. The developed method can basically be applied to a large class of combined forming settings and large numbers of parameters to be identified. However, a large part of the development of an all-round tool for virtual process design is still work in progress: So far, a complete finite element simulation of a combined forming process consisting of deep drawing and subsequent electromagnetic calibration has been implemented in an axisymmetric context and two parameters of the triggering current of the tool coil have been identified simultaneously in good quality. Although the work performed so far represents only a beginning, it already led to an improvement in forming technology, since it helped to identify process parameters extending quasi-static forming limits. Further, since

the general framework has been set up, an extension to more complicated practical problems including larger numbers of parameters both in the preceding deep drawing operation and in the subsequent EMF step is now a technical question.

The target function f to be minimized will in the following represent the deviation from a prescribed ideal value of a certain quantity computed for the proposed parameters $\vec{\lambda} = (\lambda_1, \ldots, \lambda_n)$, e.g., the distance of the computed shape $s(x, \vec{\lambda})$ of a deformed work piece from the ideal shape $s_{opt}(x)$, measured in the sense of error squares:

$$f(\vec{\lambda}) := \frac{1}{\sqrt{meas\, S}} \left\| s(x, \vec{\lambda}) - s_{opt}(x) \right\|_2 := \left(\frac{1}{meas\, S} \int_S \left| s(x, \vec{\lambda}) - s_{opt}(x) \right|^2 dx \right)^{\frac{1}{2}}. \quad (1)$$

Here, S denotes a two-dimensional plane region, which $s_{opt}(x)$ is parameterized about, and $meas\, S$ its area. In case of an axisymmetric setting, S reduces to a radial ray covered by the work piece, and $meas\, S$ denotes its length. Alternatively, a finite number of test points can be introduced to validate the deviation of the formed shape determined in the finite element simulation from the ideal one:

$$f(\vec{\lambda}) := \left(\frac{1}{N} \sum_{k=1}^{N} \left| s(x_k, \vec{\lambda}) - s_{opt}(x_k) \right|^2 \right)^{\frac{1}{2}}. \quad (2)$$

A single computation of the target function requires a complete simulation of the technological process to be optimized, e.g., by the finite element (FE) method. While several commercial programs are available that provide a satisfactory simulation of deep drawing, a sufficiently accurate simulation of electromagnetic forming is still scientifically challenging. During the work of the DFG-research groups FOR443 and the DFG-project PAK343, several methods for the FE-computation of EMF have been benchmarked and compared to each other (see, e.g., [7,8,9]). In case of the optimization of an axisymmetric forming operation of deep drawing and subsequent electromagnetic calibration, combining the commercial programs ANSYS and LS-DYNA (see [4]) has turned out to be sufficient for a computation of the target function within a satisfactory degree of accuracy. Both deep drawing and EMF have been simulated in this approach. Axisymmetric situations can be treated with the numerical efforts of a 2D-problem. However, the equations of the mechanical and electromagnetic fields have to be formulated accordingly. A full 3D-simulation is planned to be implemented in future. Results of the simulated forming process (deep drawing and subsequent EMF) are displayed on the right hand side of Figure 3. In the subsequent EM calibration step only the area of combined forming in the region of biaxial stretch of the forming limit diagram is still altered, resulting in the two peaks exceeding the quasi-static forming limit curve. The points with compression along one axis remain at the positions they reached after deep drawing. Comparison to experimental data (left hand side of Figure 3) reveals some discrepancies: Points with negative minor strain remain at an average at a larger distance to the quasi static forming limit curve. On the other hand, all these numerical determined data point lie in an area also covered by the experimental data points, which exhibit a large variation. Further, larger absolute values are reached in the area of biaxial stretch by the simulation. However, this affects only a few points. Further investigations will have to clarify whether this discrepancy results from an overestimation of dynamical forming limits during the EMF simulation or is related to the measurement process. Computing the target function as described above has also been done to produce the parameter study displayed in the right part of Figure 4 as well

as in the corresponding two-dimensional parameter identification process presented in this work.

For the mechanical structure a dynamic thermo-elastoviscoplastic material model is relevant as described in [10, 11]. It is coupled to the electromagnetic system in many ways, i.e., the Lorentz-force $\vec{F} = \vec{j} \times \vec{B}$, with current density $\vec{j}$ induced in the work piece and magnetic flux density $\vec{B}$, the position and the velocity of the work piece, Joule-heating, and temperature dependence of electrical conductivity. In the situation considered here, simplifications are admissible such that the coupling between the electromagnetic and mechanical subsystems finally reduces to the Lorentz-force and the current position of the work piece, making the distribution of electrical conductivity temporally varying.

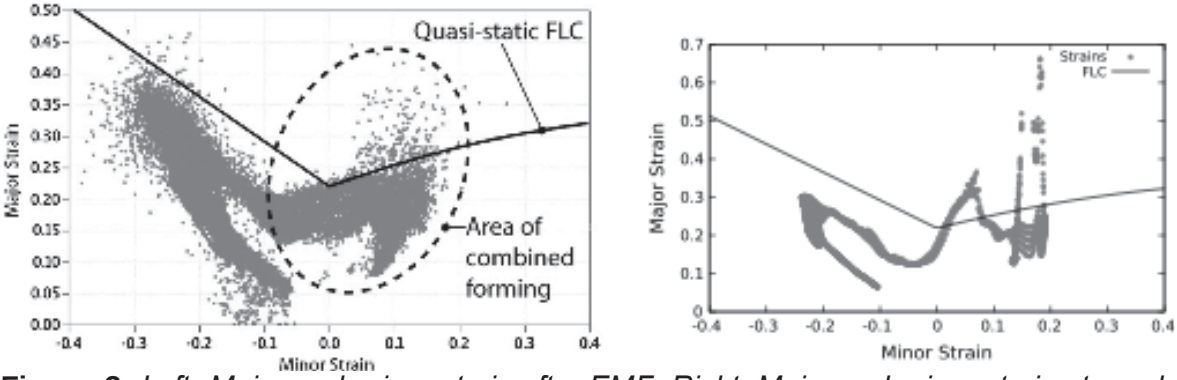

Figure 3: *Left: Major and minor strain after EMF. Right: Major and minor strain at mesh points according to the FE simulation of the combined process [4].*

There exist a couple of different optimization methods, some of which will be discussed below with regard to their advantages and disadvantages. Each of these methods provides a rule, how to search for good parameter values based on the information gained by previous computations of the target function. In addition to minimization of the target function, the optimization algorithm takes care that constraints are never violated. In the case examined here, these constraints are given by the relevant forming limits. Formally this leads to the following type of problems:

$$\begin{aligned} &minimize\ f(\lambda_1, \dots, \lambda_n) \\ &subject\ to\ c_j(\lambda_1, \dots, \lambda_n, t) \geq 0, \end{aligned} \tag{3}$$

with a parameter vector $\vec{\lambda} = (\lambda_1, \dots, \lambda_n)$ and constraints represented by $c_j(\lambda_1, \dots, \lambda_n, t)$ at time t. The functions c_j with $1 \leq j \leq m$ depend on the distance to the forming limit in strain space at time t for a set of m "critical" control points. This distance has to be positive for all t. In the subsequent section, the constraints will be modeled by functions

$$c_j(\vec{\lambda}, t) = dist\Big(\big(\varepsilon_1(\vec{\lambda}, t), \varepsilon_2(\vec{\lambda}, t)\big), \partial F_t\big(\varepsilon_1(\vec{\lambda}, t), \varepsilon_2(\vec{\lambda}, t)\big)\Big), \tag{4}$$

with $\partial F_t\big(\varepsilon_1(\vec{\lambda}, t), \varepsilon_2(\vec{\lambda}, t)\big)$ denoting the locus of material failure in strain space. Further $\varepsilon_1(\vec{\lambda}, \mathrm{t})$ and $\varepsilon_2(\vec{\lambda}, \mathrm{t})$ are the first and the second Eigenvalue of the true strain computed via

finite-element-simulation for the parameter vector $\vec{\lambda}$ at time t. In Figure 4, a two-parameter optimization of a typical forming situation is presented: The tool coil is integrated in the punch, wound around it several times, as presented on the left hand side of Figure 4. After the punch stroke, the tool coil is excited by the discharging current of a capacitor bank. This leads to a pulsed loading of this area predominantly in radial direction, strongly accelerating the area of the work piece close to the coil. The right hand side of Figure 4 shows the target function in Equation (2) as a function of the parameters angular frequency ω and the amplitude I_0 of the triggering current

$$I(t) = I_0 e^{\beta t} \cos(\omega t + \varphi) \tag{5}$$

of the tool coil. The optimization method is searching for the parameter values (ω, I_0) minimizing f. It can be seen that in the examined area many local minima of the target function lie close together. This makes the optimization problem difficult. Identification of these two parameters has been chosen as a first test example. Our further plans include optimizing the coil geometry as well as the number of coil windings, which have been determined experimentally in the examples presented in this work. Up to now, the mathematical optimization is only performed for the EMF parameters. This would be sufficient if the observations in [3] are true for larger classes of forming operations: Then, the quasi-static forming step can be adjusted such that the quasi-static forming limit is reached and the afterwards performed optimization of the parameters of the EMF will eventually extend the forming limit. However, in [3] only a particular two stage forming operation has been examined. We hope that an application of the here presented method to problems including parameters of both the deep drawing and the EMF process will help to clarify this interesting issue. Details of the optimization process are given in Chapter 4.

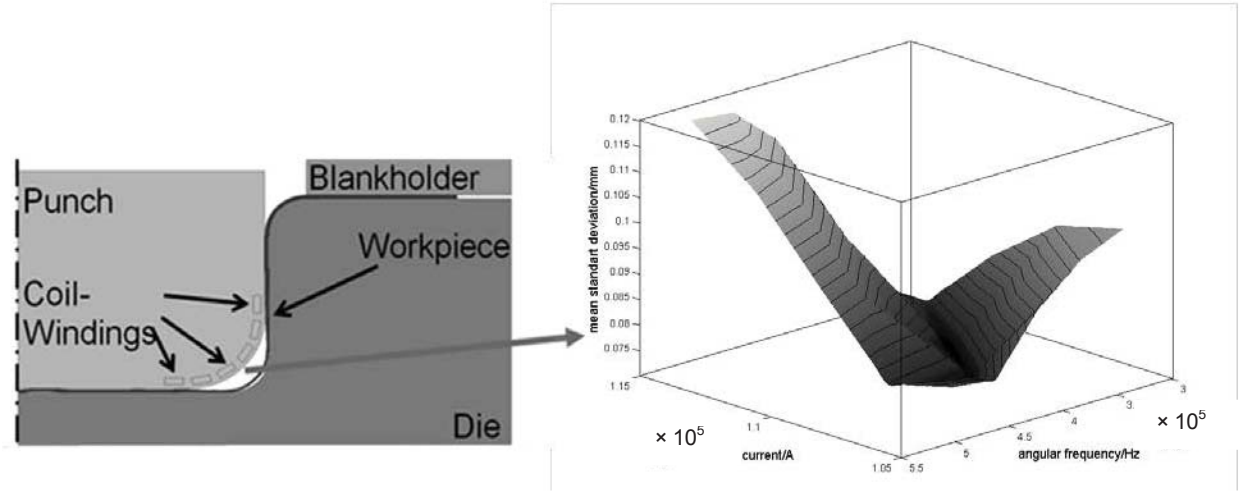

Figure 4: *Target-function landscape showing the dependence of the quality of the forming result on two input parameters for the combined process displayed on the left.*

To compute the target function in this example the axisymmetric mechanical structure is discretized by a mesh consisting of 1780 quadratic solid elements in 5 layers in each case. For the electromagnetic field computation an additional mesh in the air region between punch and forming tool has been constructed. The coupled simulation has been

carried out in 55 up to 60 time steps with a length of 1 µs each. As material, the aluminum alloy EN AA-5083 has been employed. Further details on the geometric parameters are given below.

In Figure 5, the overall organization of the optimization procedure including the optimization loop itself, the choice of initial parameters, the computation of the forming limits and its implementation as constraints, and the evaluation of the target function via a coupled finite-element simulation is displayed. Below the SQP optimization method, employed for computing the optimum parameters for the forming process displayed in Figure 4, is discussed as well as the determination of the constraints. In an earlier approach [4], the program IPOPT [12], an implementation of an interior point method, has been used.

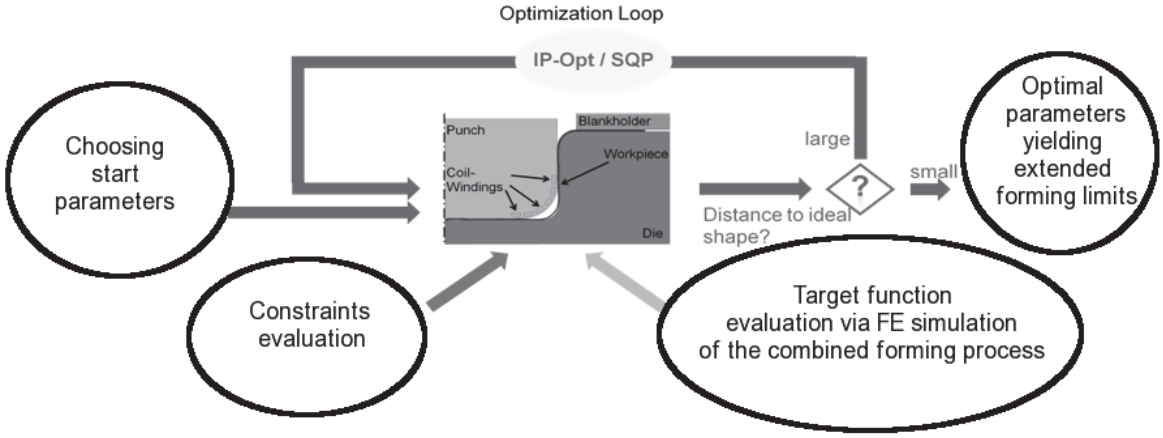

Figure 5: *Setup of the numerical optimization framework for the process combination under consideration.*

An optimization method provides a strategy to search for good values in the parameter space. While global methods gather information of the whole parameter space, local methods search better parameter values in the neighborhood of their initial values. Well known examples of global methods are evolutionary methods, such as genetic algorithms, or simulated annealing. Examples for local methods are the Nelder-Mead simplex-search ([13], see [14] for the identification of a free electromagnetic forming process of sheet metal with this method) or methods that are based on directions of descent. Very efficient methods of this type are obtained by applying algorithms for quadratic programming to second order approximations of the target function and the constraints, as done in the SQP-method (sequential quadratic programming, see below). Another type of descent methods is based on so called interior-point (IP) methods. Both IP-methods and the SQP-method require much less function evaluations to find a local minimum nearby than other methods. The reason for this is that they are more directed than the global methods mentioned above by utilizing the broader information provided by a direction of descent. However, to compute such directions of descent, a linearization of the target function is required. For the optimization of technological processes, a consistent linearization of its analytical description is not appropriate. First, this requires very complicated computations including second order derivatives of the stress-strain-relation employed in the material description. Second, a consistent linearization would only be valid for an individual pro-

cess. Therefore, the optimization method would not be robust in the sense that it applies reliably to a large class of forming processes. Hence, linearizations of the process description with respect to the parameters are here computed numerically. The SQP-method, utilized to find the minimum of the target function displayed on the right hand side of Figure 4, is based on the idea to solve a sequence of quadratic sub-problems in order to determine the descent direction in every step. These quadratic programs take the form

$$\begin{aligned} &\min_{\vec{d}} \mathcal{L}(\vec{\lambda}_k,\vec{\xi}_k) + \nabla\mathcal{L}(\vec{\lambda}_k,\vec{\xi}_k)^T\vec{d} + \frac{1}{2}\vec{d}^T\nabla^2_{\lambda\lambda}(\vec{\lambda}_k,\vec{\xi}_k)\vec{d} \\ &s.t. \quad \vec{c}(\vec{\lambda}_k) + \nabla\vec{c}(\vec{\lambda}_k)^T\vec{d} \geq 0, \end{aligned} \tag{6}$$

for every iteration k. Here

$$\mathcal{L}(\vec{\lambda},\vec{\xi}) = f(\vec{\lambda}) - \vec{\xi}^T\vec{c}(\vec{\lambda}) \tag{7}$$

denotes the Lagrangian and $\vec{\xi}$ a vector of Lagrangian multipliers. The constraints have been gathered to the vector $\vec{c}(\vec{\lambda}) = (c_1(\vec{\lambda}),\dots,c_m(\vec{\lambda}))^T$. With every solution of Equation (6) a search direction $\vec{d}$ is calculated. Then, a one-dimensional minimum along this direction is determined. This can be considered as a Newton step in order to optimize the target function f. Here, the implementation of the SQP-method provided by MATLAB [15] has been employed. To organize the whole optimization framework as shown in Figure 4, various software components have to be linked, such as LS-DYNA, ANSYS, and MATLAB. This has been achieved by extensive scripting techniques, which have been implemented in the scripting language Ruby here.

The derivatives of the target function with respect to the parameters to be identified required for a gradient based optimization method are computed numerically in this work. It has often been argued that numerically determined derivatives are not sufficiently accurate for mathematical optimization algorithms. Indeed, as an inverse problem, optimization problems are often badly conditioned. On the other hand, the decrease of the target function during optimization is monitored. Further, if the applied method of descent does not yield further improvement, simulation data, such as mesh-size or step-size for the determination of numerical derivatives can be adapted a posteriori by the algorithm. In future implementations it is also planned to choose the model for the determination of the constraints, i.e., the forming limits, adaptively: An algorithmic control of numerical parameters and of the accuracy of the employed model formulation, based on data collected during the optimization process, will then lead to increased efficiency without reducing the accuracy of the identified optima. Further, it makes the optimization scheme more robust in the sense, that a larger class of problems can be treated without cumbersome adaptations. As an example for an adaptive choice of different models - which is, however, not implemented, yet - consider the situation displayed in Figure 6: Two different models are assumed exemplarily, which can be chosen algorithmically according to the numerical needs: a damage model as provided by Lemaitre (see [16]) and the forming limit surface (FLS) discussed in the subsequent section (see Figure 7), representing a less precise, but computationally fast way to incorporate forming limits as constraints. Far away from the minimum the fast method is used while close to the area of the minimum the precise, but costly constraints are applied.

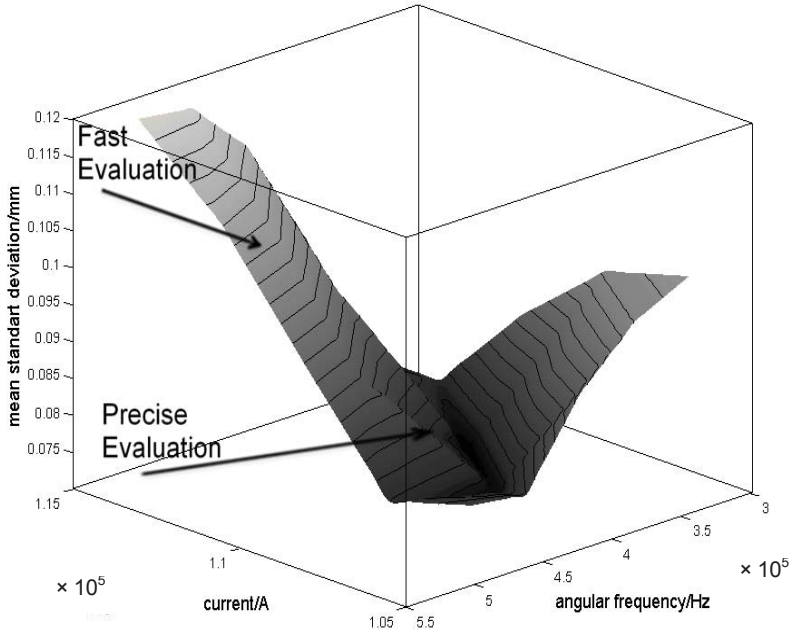

Figure 6: *The target function for two parameters: The adaptive choice of constraints takes place in the marked regions of the target function surface. Far away from the minimum the fast evaluation method with the FLS is chosen, close to the minimum a costly but accurate damage model is applied.*

The development of auto-adaptive methods of this type represents work in progress. A significant increase in efficiency is gained by computing all function values required for the linearization in parallel. If sufficient computational resources are available, even more evaluation of the target function can be carried out in parallel at the same time allowing for the determination of higher order approximations to the required derivatives.

3 Dynamic Forming Limits as Constraints in Optimization

The above described optimization methods require an efficient way to determine the relevant forming limits for each load path resulting from the particular choice of parameters due to the optimization method. This, however, requires a fast accessible computational method to estimate the distance to the point of material failure at any stage of the currently active load path considering the current strain rate. There are two well-known methods to obtain this information: The use of a damage model with identified model parameters or the use of forming limit diagrams. The first alternative, on the one hand, is in many cases too time-consuming. Usually, a set of damage variables is introduced and their evolution is tracked by a system of Gauss-point-based ordinary differential equations to be solved any time the material model is evaluated in the finite-element-simulation. Such models are, e.g., the Gurson-Nedleman-Tvergard- or the Lemaitre-model [16]. A classical forming limit diagram (FLD), on the other hand, is neither able to account for the material's load history during the forming process nor the dependence of the material's response on the

strain rate. Hence, conventional FLDs are not suited to predict forming limits of combinations of deep drawing and electromagnetic forming. To obtain a sufficiently fast method that can efficiently be incorporated in the SQP- or IP-method, that accounts for strain history and strain rate dependence, the classical FLD can be extended to a forming limit surface (FLS) [4,17,18]. To represent the relevant forming limits for a process combination of, e.g., a quasi-static and an impulse forming method, a third axis is added to a classical FLD. On this third axis, in addition to major and minor strain a parameter is considered that may represent the accumulated strain in a critical region of the work piece at the instant of switching from the quasi-static to the dynamical process. The forming limit curve corresponding to this amount of accumulated strain and the strain rate of the subsequent impulse forming operation is inserted for this parameter. Figure 7 shows such a forming limit surface. It allows for consideration of prestrain and rate dependence in the second forming step.

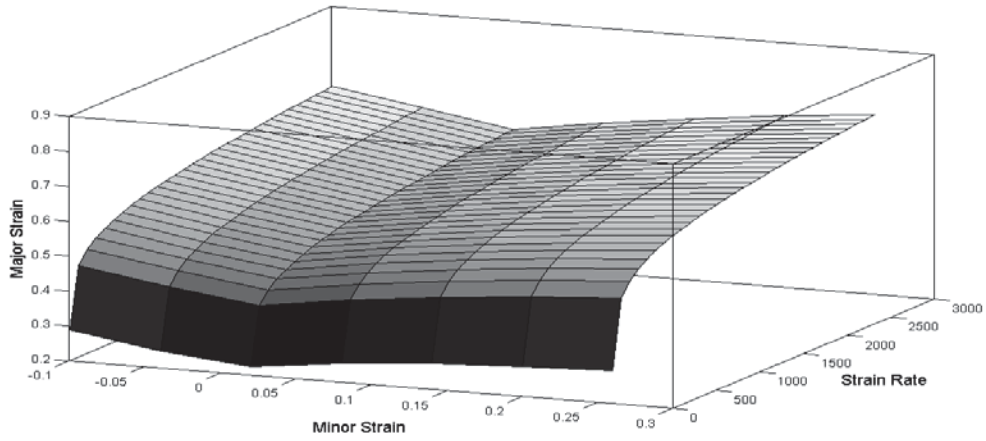

Figure 7: *The forming limit surface (FLS). The distance of the major strain as a function of minor strain and strain rate to the surface acts as a constraint in the optimization.*

The most direct way to construct an FLS is to experimentally determine forming limit curves (FLCs) at different strain rates and a certain state of previously accumulated strain. Hence, accumulated strain is automatically considered in a correct way. For such measurements, a high speed Nagazima test can be performed after previous deep drawing. From the measurement results, the FLS is then constructed by a mathematical approximation technique, e.g., least-square-approximation by two-dimensional spline functions. In a case where sufficient experimental information was not available, in [4] an FLS has been derived from a quasi-static FLC with the help of a modified Johnson-Cook type failure model (see [19]) presented and identified by Clausen et al. [20]. For further information on FLSes, see [4].

4 Results and Experimental Validation

The efficiency of the presented method has been proved in several practical situations [4]. A significant improvement of the target function value could be obtained by use of the numerical method compared to a purely experimental identification of parameter values. The

numerical computations and accompanying experiments have been carried out for sheet metal discs of 130 mm diameter and a thickness of 1 mm. The drawing distance amounts to 55 mm and the drawing radius to 10 mm. The blank holder force is set to 300 kN. These values have also been chosen for computing the target-function-landscape displayed in Figure 4 and Figure 6. Material data of EN AA-5083 have been employed, and the punch's bottom radius has been set to r = 20 mm. The blank holder force and the friction (a Coulomb-friction model with a friction factor μ = 0.04 in the flange region and μ = 0.0 elsewhere) were set to a value that would lead to material failure in a single deep drawing process. The goal was now to manufacture a part without failure, but with strains at the punch's bottom radius, exceeding the conventional forming limits due to stretching. By a preceding experimental study, the optimum number of coil winding was experimentally identified as N = 6. While in [4] ω, φ and β in the representation of the input current

$$I(t) = I_0 e^{\beta t} \cos(\omega t + \varphi), \quad with\ \omega = 3.8007 \cdot 10^5 s^{-1}, \varphi = -1.35381\ rad,\ \beta = -15467.3 s^{-1}, \tag{9}$$

have been taken from measurements, in the current work, only φ and β have been prescribed and both ω and I_0 have been simultaneously identified by a two-parameter optimization. Looking at Figure 4 and Figure 6 reveals that it was a challenging task for the optimization method to find the correct local minimum belonging to the optimum value of the target function. While for the fixed value $\omega = 3.8007 \cdot 10^5 s^{-1}$ the experimentally identified optimum for I_0 was 101 533 kA, we obtain a smaller deviation between simulated shape and ideal shape for the simultaneously identified values $\omega \approx 3.8485 \cdot 10^5 s^{-1}$ and $I_0 \approx 110\,000$ kA. Clearly, the simultaneous identification of two parameters leads to better results than their successive identification.

5 Conclusions

In this paper a method for the computer aided design of process chains consisting of classical quasi-static processes and EMF has been discussed in order to increase the classical quasi-static forming limits. The use of an optimization scheme (here the SQP-method) based on a parallelly computed direction of descent renders the challenging task of computational optimization of process chains feasible. A forming limit surface was introduced to account both for the effects of strain rate and of accumulated strain during the first quasi-static forming operation, which cannot be covered by a classical forming limit diagram. The information of the forming limit surface has been provided as constraints within the SQP method. The optimization method has successfully been applied to determine optimal parameters for a two-stage process chain proposed by [3]. In contrast to previous approaches, two parameters have been optimized at the same time. Hence, the existing results could be enhanced, and parameters for a larger extension of classical forming limits have been determined. The next steps are now

- to provide systematically measured experimental data for the construction of FLSes,
- application of the method to problems with more than two parameters to be identified simultaneously,
- to compare the FLS-approach to represent material constraints with a more accurate one based on a damage model, and

- to increase efficiency and accuracy by an algorithmic adaptive choice of the mesh- and the model.

Moreover, some questions to materials science have to be answered:

- Do different load paths activate different microscopic damage-mechanisms?
- In how far do these interact with respect to resulting macroscopic failure?
- Which type of phenomenological damage model is adequate under this type of "mixed loading"?

Finally, such methods as presented here will enable the virtual design of technological processes. This becomes an increasingly viable alternative to a purely experimentally based process layout. It decreases the number of experiments required, and hence, reduces time and costs. In many industrial areas such as the automotive industry [21], these methods are nowadays being employed. Product-Lifecycle-Management [22, 23, 24] can be considered as another example. The methods described in this work lead to a powerful implementation of this future industrial design concept.

References

[1] *Psyk, V.; Beerwald, C.; Henselek, A.; Homberg, W.; Brosius, A.; Kleiner, M.:* Integration of electro-magnetic calibration into a deep drawing process of an industrial demonstrator part. Key Engineering Materials 344, 2007, p. 435-442.

[2] *Daehn, G. S.:* High-velocity metal forming, 2006.

[3] *Vohnout, V. J.:* A Hybrid Quasi-Static / Dynamic Process for Forming Large Sheet Metal Parts From Aluminum Alloys. PhD thesis, The Ohio State University, 1998.

[4] *Taebi, F.; Demir, O. K.; Stiemer, M.; Psyk, V.; Kwiatkowski, L.; Brosius, A.; Blum, H.; Tekkaya, A. E.:* Dynamic forming limits and numerical optimization of combined quasi-static and impulse metal forming. Computational materials Science 54, 2012, p. 293-302.

[5] *Psyk, V.; Risch, D.; Kinsey, B. L.; Tekkaya, A. E.; Kleiner, M.:* Electromagnetic forming - A review. J. Mat. Proc. Techn., 2011, p. 787-829.

[6] *Silva, M. B.; Alves, L. M.; Alves, M. L.; Martins, P. A. F.:* Fracture Forming Lines in Single Point Incremental Forming. In Proc. Int. Conf. IDDRG 2010, Graz, Austria, 2010, p. 451-460.

[7] *Kleiner, M.; Brosius, A.; Blum, H.; Suttmeier, F.-T.; Stiemer, M.; Svendsen, B.; Unger, J.; Reese, S.:* Benchmark problems for coupled electromagnetic-mechanical metal forming processes. Annals of the German Acad. Soc. for Prod. Eng. WGP 11(1), 2004, p. 85-90.

[8] *Stiemer, M.; Unger, J.; Svendsen, B.; Blum, H.:* Algorithmic formulation and numerical implementation of coupled electromagnetic-inelastic continuum models for electromagnetic metal forming. International Journal for Numerical Methods in Eng. 68(13), 2006, p. 1301-1328.

[9] *Stiemer, M.; Unger, J.; Blum, H.; Svendsen, B.:* An arbitrary Lagrangian Eulerian approach to the three dimensional simulation of electromagnetic forming. Comp. Meth. Appl. Mech. Engrg. 198(17-20), 2009, p. 1535-1547.

[10] *Svendsen, B.; Chanda, T.:* Continuum thermodynamic modeling and simulation of electromagnetic forming. Technische Mechanik 23, 2003, p. 103-112.

[11] *Svendsen, B.; Chanda, T.:* Continuum thermodynamic formulation of models for electromagnetic thermoinlastic materials with application to electromagnetic metal forming. Cont. Mech. Thermodyn. 17, 2005, p. 1-16.
[12] *Wächter, A.; Biegler, L. T.:* On the implementation of a primal dual interior point filter line search algorithm for large-scale nonlinear programming. Math. Prog., 106(1), 2006, p. 25-57.
[13] *Nelder, J. A.; Mead, R.:* A simplex method for function minimization. Computer J. 7, 1965, p. 308-313.
[14] *Blum, H.; Stiemer, M.; Suttmeier, F. T.; Svendsen, B.; Unger, J.:* Coupled finite element simulation of electromagnetic sheet metal forming. In 2. Kolloquium Elektromagnetische Umformung. Forschergruppe "Untersuchung der Wirkmechanismen der elektromagnetischen Blechumformung", 2003.
[15] MATLAB 2010b, MathWorks, Natick, MA, 2010.
[16] *Lemaitre, J.; Chaboche, J.-L.:* Mechanics of solid materials. Cambridge University Press, 1990.
[17] *Taebi, F.; Demir, O. K.; Stiemer, M.; Psyk, V.; Brosius, A.; Blum, H.; Tekkaya, A. E.:* Computational Design and Forming Limits of Process Chains Composed of Quasi-Static and Dynamic Processes. In: Proceedings of the 10th International Conference on Technology of Plasticity (ICTP), Aachen, 2011.
[18] *Stiemer, M.; Brosius, A.; Tekkaya, A. E.:* Leichtbau und hochfeste Werkstoffe fordern die Umformtechnik heraus. MaschinenMarkt 37, 2011, p. 24 – 27.
[19] *Johnson, G. R.; Cook, W. H.:* Fracture characteristics of three metals subjected to various strains, strain rates, temperatures and pressures. Eng. Fracture Mechanics 21(1), 1985, p. 31-48.
[20] *Clausen, A. H.; Børvik, T.; Hopperstad, O. S.; Benallal, A.:* Flow and fracture characteristics of aluminum alloy AA5083-H116 as function of strain rate, temperature and triaxiality. Mat. Sci. and Eng. A 364, 2004, p. 260-272.
[21] *Meinhardt, J.; von Wurmb, I.:* Methodenplanung im Spannungsfeld zwischen Entwicklung und Produktion. In Bestform in Blech, 2004, p. 31-36.
[22] *Spur, G.; Krause, F.-L.:* Das virtuelle Produkt-Management der CAD Technik. Carl Hanser Verlag, 1997.
[23] *Krause, F.-L.; Jansen, H.; et al.:* Modules and tools for virtual product realization. In Proc. IX. Internationales Produktionstechnisches Kolloquium (PTK), 1998, p. 281-296.
[24] *Lee, K.:* Principles of CAD/CAM/CAE Systems. Addison Wesley, 1999.